Proceedings of the 26th Annual International Conference of the IEEE EMBS
San Francisco, CA, USA • September 1-5, 2004

Local Field Potential Measurement with Low-Power Analog Integrated Circuit

Reid R. Harrison[1], Gopal Santhanam[2], and Krishna V. Shenoy[2,3]
[1]Department of Electrical and Computer Engineering, University of Utah, Salt Lake City, Utah, USA
[2]Department of Electrical Engineering, [3]Neurosciences Program, Stanford University, Stanford, California, USA

Abstract—**Local field potentials (LFPs) in the brain are an important source of information for basic research and clinical (i.e., neuroprosthetic) applications. The energy contained in certain bands of LFPs in the 10-100 Hz range has been shown to correlate with specific arm movement parameters in non-human primates. In the near future, implantable devices will need to transmit neural information from hundreds of microelectrodes, and transcutaneous data transfer will become a significant bottleneck. Here we present a low-power, fully-integrated circuit that performs on-site data reduction by isolating LFPs and measuring their signal energy. The resulting analog VLSI circuit consumes 586 µm × 79 µm of silicon area and dissipates only 5 nanowatts of power. We show that the chip performs similarly to state-of-the-art signal processing algorithms.**

Keywords—**Local field potentials, integrated circuit, neural recording, low-power circuit design, neural prosthesis**

I. Introduction

With the advent of microelectrode arrays (for example, [1],[2]) and integrated electronics, fully-implanted neural recording devices for research and clinic applications (e.g., neuroprosthetics) are becoming a reality. With this miniaturization comes a challenge: massively-parallel neural recording systems generate huge quantities of data that must be relayed out of the body in real time. For example, a 100-channel system that digitizes each channel at a rate of 30 kSamples/sec (typical for neural recording systems) at an accuracy of 10 bits per sample gives a data stream of 30 Mbits/sec. By comparison, the FCC-approved Medical Implant Communication System (MICS) band at 402-405 MHz consists of 10 channels each with only 300 kHz of bandwidth.

This "transcutaneous data bottleneck" presents a significant technological challenge since through-the-skin cables are undesirable for cosmetic, convenience, and health reasons. We propose that data compression within the implanted device is an essential (and previously overlooked) element in a practical neural recording system. In [3], we presented the first circuit to address this problem – a low-power adaptive spike detection circuit that automatically measures the background noise level for each channel and sets a detection threshold well above the noise. The circuit was fully integrated in a commercial CMOS VLSI process.

Spikes are not the only source of information in an extracellular neural recording. Local field potentials (LFPs) are low-freqeuncy (<100 Hz) oscillations resulting from the synchronous firing of many neurons relatively close to the electrode, but too distant for individual spikes to be resolved [4]. The energy of LFP signals in primate pre-motor and motor cortex have been shown to correlate with specific arm movement reach parameters such as direction, distance, and speed, and thus may be useful in neuroprosthetic applications [5-10]. LFPs are a robust signal. In some experiments using electrode arrays, scar tissue forms around microelectrode tips. This scar tissue tends to attenuate spike signals from nearby neurons, but LFP signals are less affected [11].

In this paper, we present a fully-integrated, low-power circuit for measuring the energy present in LFP signals within a specified frequency band. In an implantable neural recording system, each electrode could have a dedicated LFP energy detection circuit. The signal produced by this circuit could then be digitized by an analog-to-digital converter at a slow rate, perhaps 10 samples per second. This greatly reduces the amount of data that must be transmitted out of the body over an RF link or other communication channel. Low power operation is vitally important for implanted systems since small levels of chronic heat dissipation (80 mW/cm^2) can lead to tissue damage [12].

II. LFP Energy Detection Algorithm

Fig. 1 presents a diagram of our LFP energy detection algorithm. To measure the energy in an LFP signal, we first use a bandpass filter to isolate the frequencies of interest. Most LFP signals of interest fall in the range of 10-100 Hz, and it is often useful to isolate a one-octave band within this range (e.g., 20-40 Hz, 40-80 Hz) [8,9,11]. Bandpass filtering also eliminates low-frequency (<10 Hz) microphonic signals due to movement and high-frequency (>100 Hz) signals from spikes.

The filtered signal is then squared, and the squared signal is passed to a leaky integrator that effectively calculates a "running average" of signal energy within the pass band of the system. The time constant of the leaky integrator determines "persistence of memory" in this running average.

This work was supported by a National Science Foundation CAREER award (ECS-0134336, R.R.H.), an NDSEG fellowship (G.S.), and the following awards to K.V.S.: NSF Center for Neuromorphic Systems Engineering at Caltech, ONR Adaptive Neural Systems, Whitaker Foundation, Center for Integrated Systems at Stanford, Sloan Foundation, and Burroughs Wellcome Fund Career Award in the Biomedical Sciences. Please address correspondence to harrison@eng.utah.edu.

0-7803-8439-3/04/$20.00©2004 IEEE

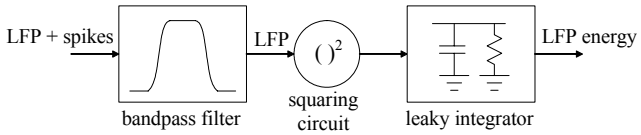

Fig. 1. Block diagram of the LFP energy detector.

III. Circuit Design and Implementation

We designed the LFP energy detector for implementation in a CMOS integrated circuit with the goal of minimizing power consumption and chip area. All transistors were operated in the subthreshold region to conserve power and achieve large time constants with integrated capacitors [13]. We used a 5 V power supply.

A schematic of the bandpass filter is shown in Fig. 2. The circuit uses five operational transconductance amplifiers (OTAs) and seven capacitors to realize a fourth-order bandpass filter. We use the standard technique of stagger tuning where two second-order bandpass filters are cascaded and tuned to slightly different frequencies. The combination of their transfer functions results in a wider, flatter pass band than in either single filter.

Each second-order bandpass filter consists of two operational transconductance amplifiers (OTAs) and three capacitors. The OTAs use diode-connected transistors for source degeneration to extend their linear range. The transfer function of each filter is given by

$$\frac{v_{OUT}(s)}{v_{in}(s)} = -\frac{AN}{\beta}\cdot\frac{\left(1-\frac{s}{\omega_0\beta}\right)}{\frac{s}{\omega_0}+\frac{1}{Q}+\frac{\omega_0}{s}} \quad (1)$$

where

$$\omega_0 = 2\pi f_0 = \frac{g_m}{\beta C} \quad (2)$$

$$\beta = \sqrt{N(A+1)(K+1)-N} \approx \sqrt{NAK} \quad \text{if } A,K >> 1 \quad (3)$$

$$Q = \frac{\beta}{(K+N)} \quad (4)$$

The output signal v_{OUT} is centered around V_{REF}, a dc voltage which was set to 1.2 V. We sized the capacitors in our circuit to give $A = 20$ and $K = 5$ (with $C = 0.1$ pF). The transconductance of the lower OTA was set by adjusting its bias current I_B:

$$g_m = \frac{\kappa}{(\kappa+1)}\cdot\frac{I_B}{2U_T} \quad (5)$$

where κ is the weak inversion slope (approximately 0.7) and U_T is the thermal voltage kT/q (approximately 26 mV at room temperature). We set the bias current in the upper OTA five times smaller to achieve $N = 5$.

As we see from (1), this circuit acts as an ac-coupled second-order bandpass filter centered at f_0 with a quality factor Q set to 2.5 by capacitor and bias current ratios. The circuit also has a zero at βf_0, but since $\beta = 25$ in our circuit, the zero takes effect outside that passband and thus has little practical effect on the filter. We added a single-pole lowpass filter to the circuit (center OTA in Fig. 2) to ensure that the gain decreases at high frequencies despite the presence of this zero.

We used a bias current of I_B = 43 pA and 24 pA in the lower OTAs and 8.8 pA and 4.8 pA in the upper OTAs to center the pass bands of the first and second bandpass filters near 36 Hz and 22 Hz, respectively. The combined system has a pass band from 20-40 Hz with a two-pole (40 dB/decade) roll-off at each end.

Fig. 3 shows a schematic of the circuit that squares the signals from the bandpass filter and produces a running average of signal energy. We use a subthreshold CMOS Gilbert multiplier to square the input voltage v_{LFP} provided by the bandpass filter. The output of the Gilbert multiplier is a bidirectional current (due to the nMOS current mirror) that is forced into an OTA configured as a g_m-C filter ($g_{m\text{-}int}$ and C_{int} in Fig. 3). The time constant of this filter was set to 100 ms, a reasonable value for the integration of LFP signal energy in the 20-40 Hz range.

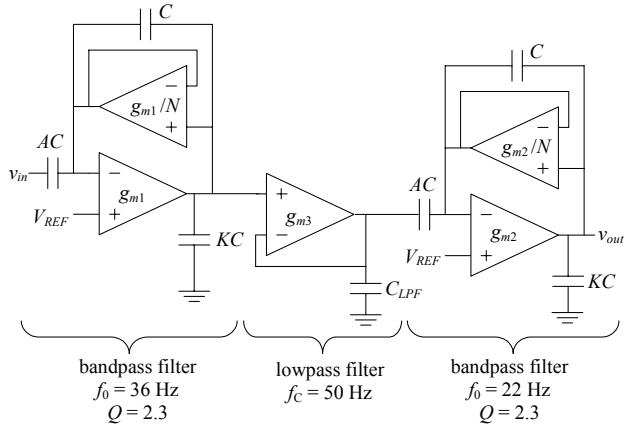

Fig. 2. Schematic of stagger-tuned 4th-order bandpass filter tuned for a one-octave passband of 20-40 Hz.

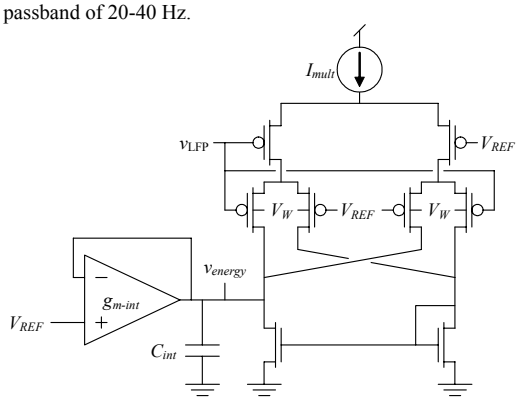

Fig. 3. Schematic of circuit to square v_{LFP} signal and perform a leaky integration to produce a "running average" of LFP energy v_{energy}.

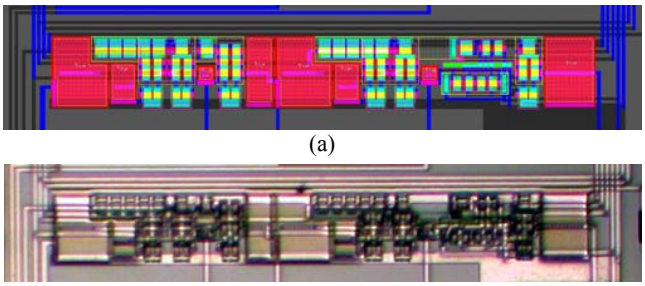

(a)

(b)

Fig. 4. (a) Layout of LFP energy detector circuit. (b) Microphotograph of the circuit after fabrication in a standard 1.5-µm CMOS process. The circuit measures 586 µm × 79 µm.

IV. Results

A. Fabrication and Biasing

The LFP energy detection circuit was fabricated in a commercially-available 1.5-µm 2-metal, 2-poly CMOS process through the MOSIS service. The circuit was completely integrated, using no off-chip components. The circuit contained eight capacitors with a total capacitance of 8.2 pF. The LFP detector layout consumed a chip area of 586 µm × 79 µm (0.046 mm^2), and is shown in Fig. 4a. A microphotograph of the fabricated circuit is shown in Fig. 4b. Capacitors consume approximately 50% of the layout area.

The bandpass filter was biased to have a pass band of approximately 20-40 Hz. A network analyzer was used to measure the filter transfer function (see Fig. 5). As expected, the filter exhibits a 40 dB/decade roll-off outside of the pass band of 21-40 Hz. The filter has a midband gain of approximately 26 dB. To demonstrate the tunable nature of the circuit, the transfer function was also measured with the bias currents doubled, yielding a pass band of 39-88 Hz (right curve in Fig. 5). The pass band was set back to 21-40 Hz for all later experiments.

B. Testing with Synthetic Stimuli

We then tested the complete LFP energy detection circuit using a synthetic stimulus supplied by an Agilent 33120A function generator – an amplitude-modulated 30-Hz sine wave (see Fig. 6, top). The circuit tracks the amplitude of the oscillation (see Fig. 6, bottom). Note the ~100 ms phase lag between the peak amplitude and the peak response of the circuit. This is an unavoidable effect of using a leaky integrator to calculate a running average of signal energy.

We also tested the circuit using a constant-amplitude, frequency-modulated sine wave (see Fig. 7, top). This signal varied from 5 Hz to 55 Hz with sinusoidal modulation. The chip responds when the sine wave frequency passes through its 21-40 Hz pass band (see Fig. 7, bottom).

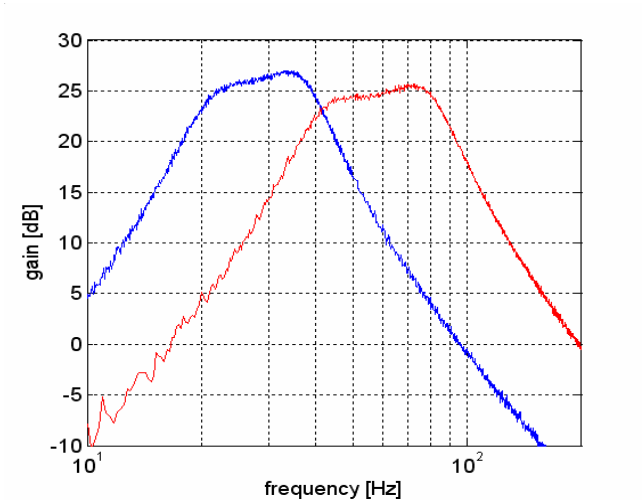

Fig. 5. Measured filter passbands for two different biasing conditions. Left curve: Passband of 21 Hz – 40 Hz used in this paper. Right curve: Increasing the filter bias currents shifts the passband to 39 Hz – 88 Hz.

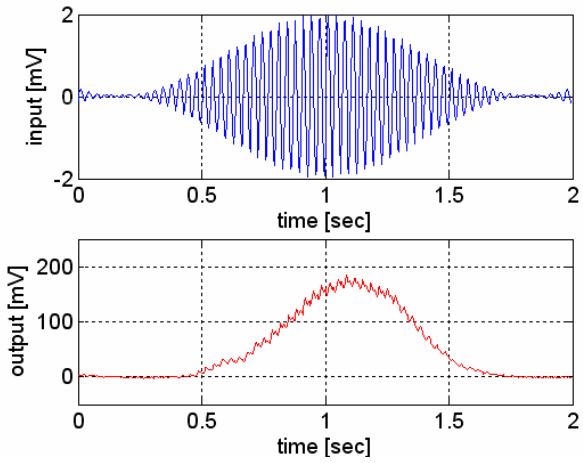

Fig. 6. Measured response of LFP energy detection circuit (bottom) to a synthetic waveform (top): amplitude-modulated 30-Hz sine wave.

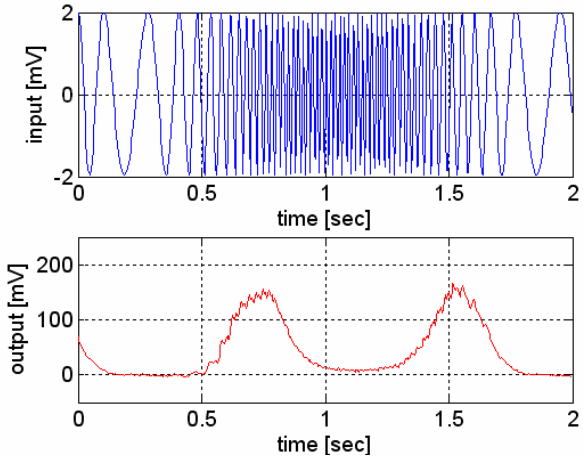

Fig. 7. Measured response of LFP energy detection circuit (bottom) to a synthetic waveform (top): sine wave frequency modulated from 5 to 55 Hz.

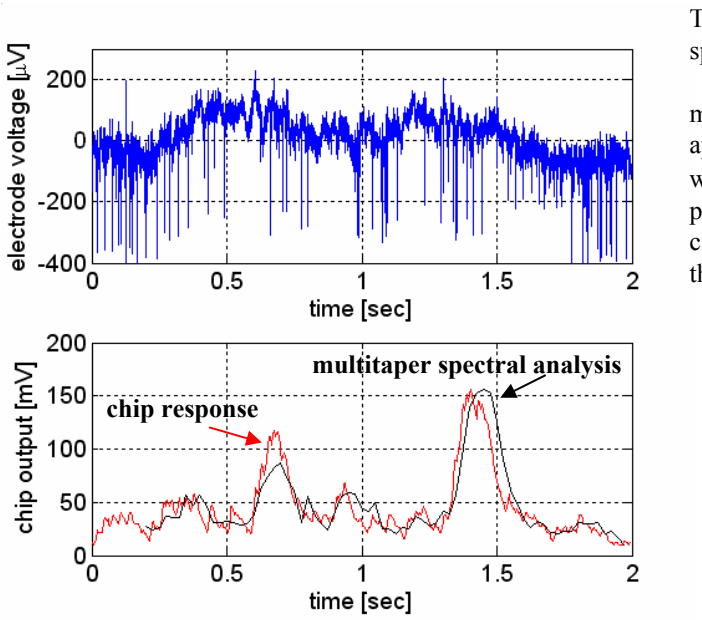

Fig. 8. Neural waveform containing spikes and local field potentials (top). Bottom graph shows the response of the LFP energy detection circuit (jagged line) compared to the response of a Thomson multitaper spectral analysis run offline on a PC (smooth, dark line). Both techniques measured LFP energy in the 20-40 Hz band.

C. Testing with Neural Data

As a final test of circuit performance, we recorded broadband neural data from a silicon-based 100-electrode array [2] chronically implanted in the pre-motor and motor cortex of a rhesus monkey (0.3 Hz – 7.5 kHz; 30 kSamples/sec, 12-bit samples). We programmed a two-second segment of neural data from one of the 100 electrodes into the function generator (see Fig. 8, top) and played it to the chip, amplified by a factor of 60 dB. (In an actual neural recording system, the LFP energy detection circuit would be connected to the recording electrode via a low-noise preamplifier such as the one described in [14].)

The chip's response was compared to a Thomson multitaper spectral analysis performed on a PC using MATLAB as shown at the bottom of Fig. 8. An arbitrary scaling factor was used to align the two curves' amplitudes. The circuit output closely follows the multi-taper analysis results, which is widely considered to be the optimal spectral analysis method for LFP analyses [8,11].

V. Conclusion

We have presented a novel circuit for the detection of local field potential oscillation energy in neural recordings. Our circuit was completely integrated in a commercially-available CMOS process. The circuit consumes a total of 5 nanowatts of power when run from a 5 V power supply. The circuit accurately detects LFP energy levels within a specified pass band.

The small size and low power operation of this circuit make it compatible with fully-implanted multi-electrode applications. As an example, 100 copies of this circuit would consume only 4.6 mm^2 of chip area in a 1.5-μm process with a power consumption of 0.5 μW. With [3], this circuit represents another tool for neural data reduction at the level of the implant.

References

[1] A.C. Hoogerwerf and K.D. Wise, "A three-dimensional microelectrode array for chronic neural recording," *IEEE Trans. Biomed. Eng.,* vol. 41, pp. 1136-1146, Dec. 1994.

[2] C.T. Nordhausen, E.M. Maynard, and R.A. Normann, "Single unit recording capabilities of a 100 microelectrode array," *Brain Research,* vol. 726, 129-140, 1996.

[3] R.R. Harrison, "A low-power integrated circuit for adaptive detection of action potentials in noisy signals," In: *Proc. 2003 Intl. Conf. of the IEEE Eng. in Medicine and Biology Soc.,* pp. 3325-3328, Cancún, Mexico, 2003.

[4] A.C. Metting van Rijn, A. Peper, and C.A. Grimbergen, "High-quality recording of bioelectric events," *Med. Biol. Eng. Comput.,* vol. 29, pp. 1035-1044, 1986.

[5] V.N. Murthy and E.E. Fetz, "Coherent 25- to 35-Hz oscillations in the sensorimotor cortex of awake behaving monkeys," *Proc. Natl. Acad. Sci. USA,* vol. 89, pp. 5670–5674, 1992.

[6] J.P. Donoghue, J.N. Sanes, N.G. Hatsopoulos, and G.Gaal, "Neural discharge and local field potential oscillations in primate motor cortex during voluntary movements," *J. Neurophysiol.,* vol. 79, pp.. 159-173, 1998.

[7] K.V. Shenoy, D. Meeker, S. Cao, S.A. Kureshi, B. Pesaran, P. Mitra, C.A. Buneo, A.P. Batista, J.W. Burdick, and R.A. Andersen, "Neural prosthetic control signals from plan activity," *NeuroReport,* vol. 14, pp. 591-596, 2003.

[8] G. Santhanam, M.M. Churchland, M. Sahani, and K.V. Shenoy, "Local field potential activity varies with reach distance, direction, and speed in monkey pre-motor cortex," *Soc. for Neuroscience, Abstracts,* 2003.

[9] K.V. Shenoy, M.M. Churchland, G. Santhanam, B.M. Yu, and S.I. Ryu, "Influence of movement speed on plan activity in monkey pre-motor cortex and implications for high-performance neural prosthetic system design," In: *Proc. 2003 Intl. Conf. of the IEEE Eng. in Medicine and Biology Soc.,* pp. 1897-1900 Cancún, Mexico, 2003.

[10] C. Mehring, J. Rickert, E. Vaadia, S. Cardoso de Oliveira, A. Aertsen, S. Rotter, "Inference of hand movements from local field potentials in monkey motor cortex," *Nature Neurosci.,* vol. 6, pp. 1253-1254, 2003.

[11] B. Pesaran, J.S. Pezaris, M. Sahani, P.P. Mitra, and R.A. Andersen, "Temporal structure in neuronal activity during working memory in macaque parietal cortex," *Nature Neurosci.,* vol. 5, pp. 805-811, 2002.

[12] T.M. Seese, H. Harasaki, G.M. Saidel, and C.R. Davies, "Characterization of tissue morphology, angiogenesis, and temperature in the adaptive response of muscle tissue to chronic heating," *Lab. Investigation,* vol. 78(12), pp. 1553-1562, 1998.

[13] C. Mead, *Analog VLSI and Neural Systems,* Reading, MA: Addison-Wesley, 1989.

[14] R.R. Harrison and C. Charles, "A low-power low-noise CMOS amplifier for neural recording applications," *IEEE J. Solid-State Circuits,* vol. 38, pp. 958-965, June 2003.